

■ Imaging Agents

Multidrug-Containing, Salt-Based, Injectable Supramolecular Gels for Self-Delivery, Cell Imaging and Other Materials Applications

Rajdip Roy and Parthasarathi Dastidar^{*[a]}

Abstract: Both molecular and crystal-engineering approaches were exploited to synthesize a new class of multi-drug-containing supramolecular gelators. A well-known non-steroidal anti-inflammatory drug, namely, indomethacin, was conjugated with six different L-amino acids to generate the corresponding peptides having free carboxylic acid functionality, which reacted further with an antiviral drug, namely, amantadine, a primary amine, in 1:1 ratio to yield six primary ammonium monocarboxylate salts. Half of the synthesized salts showed gelation ability that included hydrogelation, organogelation and ambidextrous gelation. The gels were characterized by table-top and dynamic rheology and differ-

ent microscopic techniques. Further insights into the gelation mechanism were obtained by temperature-dependent ¹H NMR spectroscopy, FTIR spectroscopy, photoluminescence and dynamic light scattering. Single-crystal X-ray diffraction studies on two gelator salts revealed the presence of 2D hydrogen-bonded networks. One such ambidextrous gelator (capable of gelling both pure water and methyl salicylate, which are important solvents for biological applications) was promising in both mechanical (rheoreversible and injectable) and biological (self-delivery) applications for future multi-drug-containing injectable delivery vehicles.

Introduction

Smart soft materials such as supramolecular gels having both biomedical^[1,2] and rheoreversible^[3] behaviour are of great interest because they are emerging as promising biomaterials for developing injectable self-delivery systems.^[1,4] In conventional drug-delivery techniques, the drug is loaded on a carrier (e.g., vesicles,^[5] reverse micelles,^[6] polymer gel matrix,^[7] virus^[8] etc.) and then delivered at the target site. Non-trivial synthetic impediments pertaining to the accessibility of the carrier molecule, efficient loading (physical or chemical) of the drug into the carrier, subsequent release of the drug at the target site, and cytotoxicity, biodegradability and biostability of the carrier molecule along with the consequential side effects are some of the crucial challenges associated with such conventional approaches.

To overcome these problems, an alternative drug-delivery system known as self-delivery is becoming popular.^[9,10] One of the approaches to developing self-delivery systems involves converting the drug/prodrugs or biogenic molecules themselves to supramolecular gelators,^[11–18] either by chemical (covalent) or supramolecular (non-covalent) modifications, so that

it can deliver itself (hence the name “self-delivery”) to the target site via an invasive (subcutaneous) or non-invasive (topical) route.

Supramolecular gelators, which are usually derived from small molecules having molecular weight less than 3000, also known as low molecular weight gelators or LMWGs,^[19–21] are capable of immobilizing a large amount of liquid within the gel network through capillary forces to result in gels. LMWGs have drawn keen attention of the materials research community because of their various potential applications such as in developing templates for crystallization,^[22] sensors,^[23] cosmetics,^[24] electrooptics/photonics,^[25] oxygen-storage materials,^[26] catalysis,^[27] conservation of art,^[28] regenerative medicine,^[29] structure-directing agents,^[30] biomineralization,^[31] wound healing,^[32] enzyme mimics,^[33] medical diagnostics,^[34] tissue engineering,^[35] inhibitors of cancer cells,^[36] immunosuppressive materials,^[37] 3D cell cultures^[38] and so on. However, designing LMWGs a priori is a daunting task because of the lack of molecular-level understanding of the gelation mechanism. Nevertheless, several groups are actively involved in developing methodologies for designing new gelators.^[39–43] It is believed widely that the gelator molecules form 1D networks sustained by various non-covalent interactions (hydrogen bonding, π - π , hydrophobic, van der Waals, charge-transfer, donor-acceptor, metal coordination, etc.). Such 1D networks are then entangled to form a 3D assemblies known as self-assembled fibrillar networks,^[44] the surface of which, if conducive, is able to immobilize the gelling solvent by capillary-force action to give a gel. We have contributed significantly to the understanding and subsequent design of LMWGs.^[45–47] In this endeavour, we have successfully employed supramolecular synthons^[48] in the con-

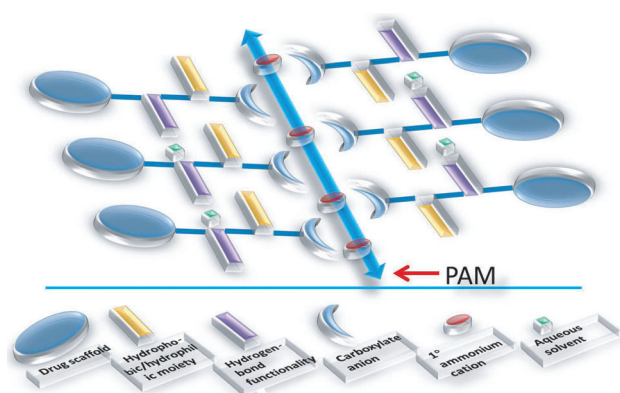
[a] R. Roy, Prof. P. Dastidar
Department of Organic Chemistry
Indian Association for the Cultivation of Science (IACS)
2A and 2B, Raja S. C. Mullick Road
Jadavpur, Kolkata 700032, West Bengal (India)
E-mail: ocpd@iacs.res.in
parthod123@rediffmail.com

Supporting information for this article can be found under <http://dx.doi.org/10.1002/chem.201602429>.

text of crystal engineering^[49] to design LMWGs capable of displaying various functional properties^[50–52] including self-delivery applications.^[53,54] We recently exploited primary ammonium monocarboxylate (PAM) synthons, which are among the most successful gel-inducing supramolecular synthons developed by us, to develop supramolecular topical gels for combination therapy.^[55]

While hydrogen-bonding among the gelator molecules is the key interaction for gel-network formation in organogels, such a self-assembly process involving gelator molecules is expected to be highly compromised in hydrogels, because the target solvent water molecules, which are both hydrogen-bond donors and acceptors, take part in hydrogen bonding and are very much part of the gel network. Thus, a critical balance between hydrophobic and hydrophilic interactions is the key to hydrogelation.^[56] Recently, we demonstrated that orthogonal hydrogen bonding^[57,58] involving amide functionality and PAM synthons played a crucial role in designing PAM salt-based hydrogelators capable of displaying various material behaviours, such as sensing ammonia and purification of dyes from water.^[59]

In the present study, we aimed to exploit such orthogonal hydrogen bonding together with hydrophobic/hydrophilic interactions to develop hydrogels/organogels for multidrug self-delivery via non-invasive (topical) and invasive (subcutaneous) routes. To this end, we considered exploiting PAM synthons with additional hydrogen-bonding functionality (amide) and hydrophilic/hydrophobic moiety on a drug scaffold (Scheme 1).



Scheme 1. Design of PAM salt-based gelators.

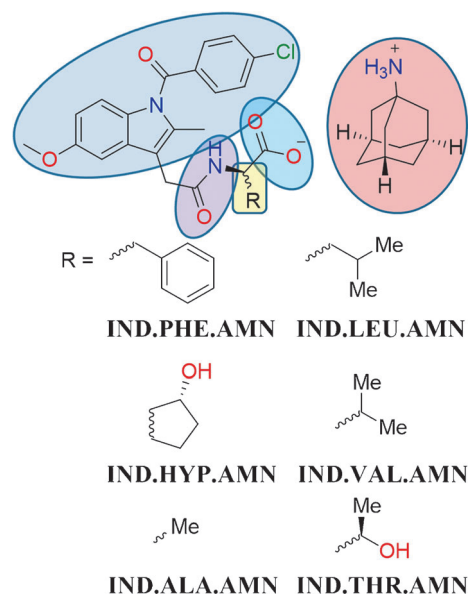
For this purpose, we first made peptide conjugates of a well-known nonsteroidal anti-inflammatory drug (NSAID), namely, indomethacin (**IND**), with some selected L-amino acids having hydrophilic [*trans*-3-hydroxy L-proline (**HYP**) and L-threonine (**THR**)] and hydrophobic [L-phenylalanine (**PHE**), L-leucine (**LEU**), L-valine (**VAL**) and L-alanine (**ALA**)] side chains. The monocarboxylic acid peptide conjugates thus synthesized reacted further with the primary amine antiviral drug amantadine (**AMN**) to generate PAM salts as potential supramolecular gelators for self-delivery applications, as described above. We deliberately chose to work with **IND** because its emission property is well known,^[60] and therefore the corresponding bioconju-

gate salts could be used for cell imaging.^[61,62] Indeed, 50% of the PAM salts thus prepared turned out to be good to moderate gelators.

Remarkably, one such gelator salt, namely, **IND-LEU-AMN**, was found to be biocompatible, anti-inflammatory and capable of cell imaging, and its hydrogel was injectable and thus suitable for self-delivery applications. Its methyl salicylate (**MS**) gel displayed interesting load-bearing and self-healing properties. To the best of our knowledge, salt-based, multidrug-containing supramolecular gels exhibiting both biological (self-delivery/cell imaging) and other materials properties (self-healing, load-bearing and shape-sustaining) have never been explored so far.

Results and Discussion

Monocarboxylic acid peptide conjugates of **IND** were prepared by following a literature procedure (see the Supporting Information, Scheme S1).^[63] The corresponding **AMN** salts were prepared by treating the peptide conjugates with **AMN** in 1:1 molar ratio in MeOH at room temperature (Scheme 2). FTIR



Scheme 2. Various salts derived from the NSAIDs indomethacin (**IND**) and amantadine (**AMN**).

data provided evidence of salt formation. The absence of the COOH stretching band ($1735\text{--}1712\text{ cm}^{-1}$) of the peptide conjugates in the spectra of the resulting salts indicated proton transfer, that is, salt formation (for a specific salt, see the Supporting Information, Figure S1). All the peptide salts thus prepared were scanned for gelation with various polar, nonpolar and aqueous solvents. Remarkably, 50% of the peptide salts, namely, **IND-PHE-AMN**, **IND-HYP-AMN** and **IND-LEU-AMN**, turned out to be gelators. Gelation was confirmed by the test-tube inversion method, whereby no gravitational flow of the gel was seen when the container was inverted. All the gels were thermoreversible over several cycles. Gelation data (for

detailed gelation studies, see the Supporting Information, Table S1 and Figures S8–S10) revealed that the amino acid side chain of the peptide conjugate salts had a profound effect on gelation. The gradual increase in the number of C atoms and consequent hydrophobicity of the amino acid side chain in these salts on going from **IND-ALA-AMN** to **IND-PHE-AMN** seemed to be influencing the gelation ability of the salts. It appeared that the critical balance between hydrophobicity and hydrophilicity was best achieved in **IND-LEU-AMN**, as is evident from its ambidextrous ability to gel both organic solvents and pure water.

The minimum gelator concentrations (MGCs) of many organogels and the hydrogel of this salt were less than 1.0 wt% and thus indicate remarkable gelation efficiency of **IND-LEU-AMN**. The fact that **IND-PHE-AMN** was able to gel mainly aromatic solvents indicated that π - π interactions perhaps helped the gelation process. The peptide conjugate salt **IND-HYP-AMN** having a polar amino acid side chain turned out to be the least versatile gelator, and was able to gel only MS. On the other hand, the peptide conjugate salts having less hydrophobic side chains (**IND-ALA-AMN** and **IND-VAL-AMN**) turned out to be non-gelators, whereas the higher hydrophilicity of **IND-THR-AMN** compared to **IND-HYP-AMN** proved to be detrimental to gelation. The gels were characterized by table-top rheology;^[64] a steady increase in the T_{gel} value with increasing concentration of the gelator indicated the importance of various supramolecular interactions such as hydrogen bonding in gel-network formation. The table-top rheology data also showed that the gels derived from **IND-LEU-AMN** were thermally more stable than those derived from the other two gelators (Figure 1).

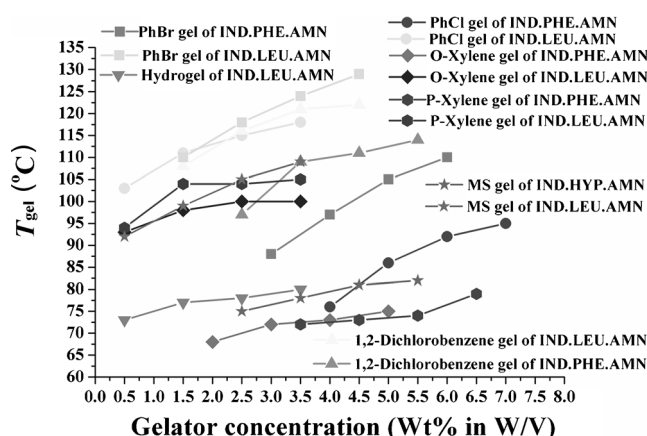


Figure 1. T_{gel} versus [gelator] plots for the gels.

Dynamic rheological experiments were carried out to evaluate the viscoelastic nature of all the gels studied herein. For this purpose, we first carried out amplitude-sweep experiments to determine the linear viscoelastic (LVE) range, which suggested the corresponding strain required for the frequency-sweep experiments. Remarkably, in all cases, the elastic modulus G' was found to be larger than the viscous modulus G'' and was

nearly frequency-invariant, indicative of the viscoelastic nature of the gels (see the Supporting Information, Figures S13–S29 and Table S6). The rheological behaviour of the MS gel and the hydrogel of **IND-LEU-AMN** turned out to be nearly identical ($G' \approx 10^5$), which suggests a remarkable ability of this ambidextrous gelator to self-assemble equally efficiently in both organic and aqueous solvents (Figure 2). The rheological behaviour

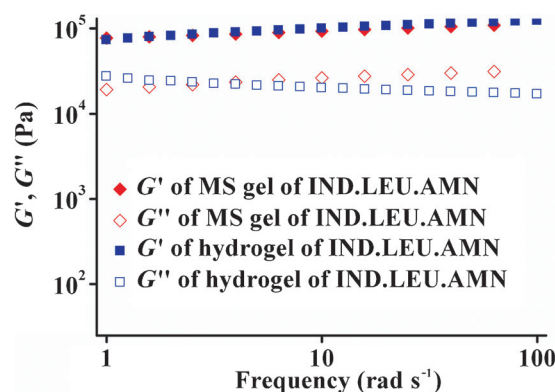


Figure 2. Frequency-sweep experiments on the hydro and MS gels.

of the hydrogel of **IND-LEU-AMN** with temperature was also evaluated under dynamic shear, and the data were in good agreement with the expected behaviour of a viscoelastic gel-like material; with increasing temperature the corresponding moduli G'/G'' gradually decreased and crossed each other at 68.5 °C, indicating gel–sol transition. The complex viscosity was also found to decrease, as expected for a more fluid-like state (see the Supporting Information, Figure S31).

We focused further rheological studies on the MS gel and the hydrogel of **IND-LEU-AMN**, because both solvents (MS and water) are important in biological applications and the gelator salt is a supergelator. Since our goal is to develop self-delivery systems for delivering the drug via invasive (subcutaneous) and non-invasive (topical) routes, and rheoreversibility of the resulting gel is an important criterion for achieving such goals, we carried out further rheological studies. For this purpose, we first evaluated the critical strains γ_c for both the MS gel and hydrogel (4 wt%) of the supergelator, which turned out to be 5.3 and 25.1 %, respectively. In separate experiments, both gels (2 mL, 4.0 wt%) were sheared at high strain (above the critical strain, 10 and 30% for MS gel and hydrogel, respectively) for 100 s and then returned to the low strain of the LVE region. Viscous response ($G'' > G'$) was observed at high strain with subsequent instantaneous recovery to elastic response ($G' > G''$) for both samples over several cycles, and this demonstrates clearly that the behaviour of the gels is rheoreversible (Figure 3).

Thus, high plateau modulus ($G' \approx 1000$ KPa), high yield stress (10 KPa) and instantaneous recovery under shear for both gels indicated that they can be used for self-delivery applications as proposed. To evaluate further the suitability of the hydrogel for invasive (subcutaneous) delivery, the injectability of the hydrogel was assessed. Preloaded hydrogel in a 5 mL hypodermic

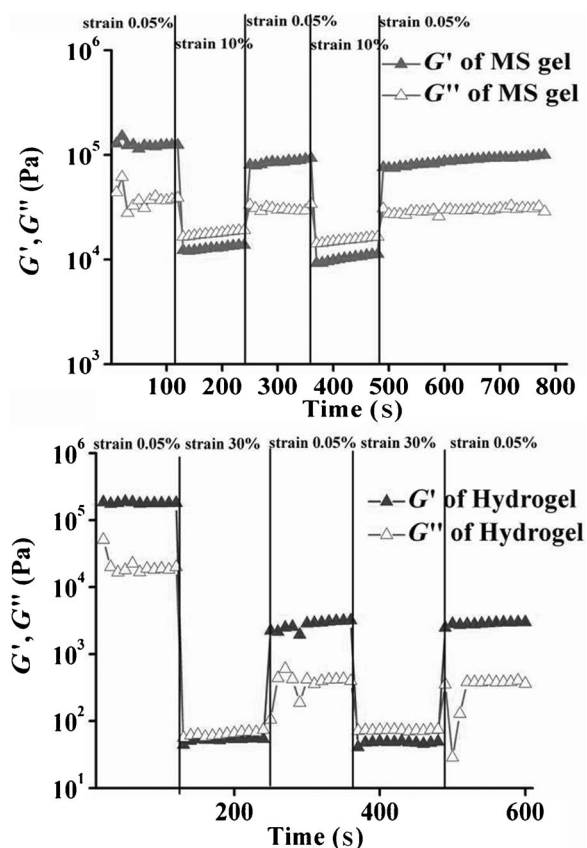


Figure 3. A 4 wt% **IND-LEU-AMN** gel in MS and in water was cycled between high and low oscillatory shear strains. First, the sample was sheared for 100 s at low amplitude of $\gamma = 0.05\%$ (proposed LVE strain) with an angular frequency of $\omega = 10 \text{ rad s}^{-1}$, which is within its LVE. For the next 100 s, the sample was transferred to high strain amplitude of $\gamma = 10\%$ and 30% for MS gel and hydrogel, respectively, with the same angular frequency of $\omega = 10 \text{ rad s}^{-1}$ which is well beyond the yield stress or LVE range. This cycle was then repeated once more.

syringe could be injected into a container as a sol, which turned into gel within a few minutes (Figure 4; for video, see the Supporting Information).

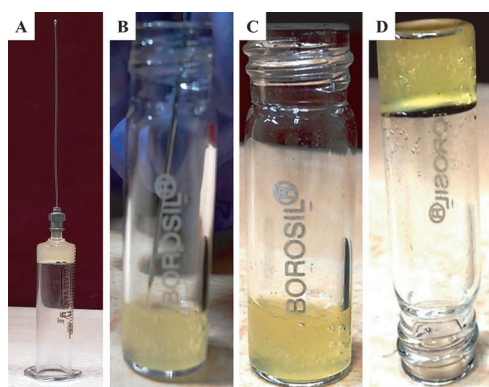


Figure 4. A) Preloaded hydrogel of **IND-LEU-AMN** in a 5 mL hypodermic syringe. B) Hydrogel flowing freely through the needle of the syringe. C) Hydrogel after passing through the syringe. D) Formation of hydrogel after a few minutes.

The rheoreversible behaviour of the MS gel also encouraged us to evaluate its self-healing, load bearing and shape-sustaining properties. A block of MS gel (4 mL, 4 wt%) was able to sustain its shape outside a container. The same block was able to hold thirteen Indian five Rupee coins (each weighing 6.7 g) amounting to 1.3 psi (8.72 kPa), beyond which the gel collapsed. Five such gel blocks, obtained by cutting a single large piece and dyed alternately with rhodamine B, were brought into contact without applying any extra force; within a few minutes, all the pieces were found to have self-healed, and the integrity of the self-healed gel block was evident from its shape sustainability when placed between two bars. These results corroborated well with the rheoreversible property described above (see the Supporting Information, Figure S35). We believe that such load-bearing, self-healing properties will be conducive to homogenous spreading of the gel in topical application.

The morphology of the gel network of some of the selected gels was studied by high-resolution TEM (HRTEM). Since MS and water are important solvents for the main focus of the present study, we selected both the MS gels and the hydrogels of **IND-HYP-AMN** and **IND-LEU-AMN**. For the other gelator **IND-PHE-AMN**, we chose to study the gels derived from chlorobenzene and *o*-xylene. For this purpose, the sample was prepared by smearing the gel (4 wt%) on a carbon-coated copper grid. 1D tapes several micrometres long, apparently composed of thin fibres, were seen for both chlorobenzene and *o*-xylene gels of **IND-PHE-AMN**. In the case of the MS gel of **IND-HYP-AMN**, a 3D network of highly entangled 1D fibres was observed. On the other hand, shorter fibres forming a 3D network by complex entanglement were observed in the case of the MS gel derived from **IND-LEU-AMN**. Interestingly, the hydrogel of the same gelator showed a 3D network composed of the thinnest fibres among the studied samples (Figure 5).

To understand the self-assembly process of hydrogelation in more detail, we carried out temperature-dependent ^1H NMR spectroscopy, which was established to be effective in explaining the role of $\text{C-H}\cdots\pi$ and $\pi\cdots\pi$ interactions^[65] in gelation mechanisms. Thus, variable-temperature ^1H NMR spectra were recorded for the hydrogel of **IND-LEU-AMN** (10 mg in 0.6 mL of D_2O). The upfield shift of both the aromatic and aliphatic protons on going from high temperature (85°C , sol) to low temperature (25°C , gel) revealed that in the gel state the self-assembled molecules were in close proximity, so that both the aromatic and aliphatic protons experience shielding by the neighbouring aromatic π -electron clouds, suggestive of $\text{C-H}\cdots\pi$ and $\pi\cdots\pi$ interactions involving the aromatic/aliphatic moieties of the salt (Figure 6). To rule out the possibility of proton shifts due to effects unrelated to the self-assembly process, we performed a control experiment wherein a D_2O solution of **IND-LEU-AMN** at a concentration of 0.3 wt% (well below the MGC of 0.5 wt%) was subjected to variable-temperature ^1H NMR spectroscopy. The data clearly showed that there was no significant shift of any of the protons (see the Supporting Information, Figure S42), which indicated that no specific self-assembly of the molecules in the sol state occurred.

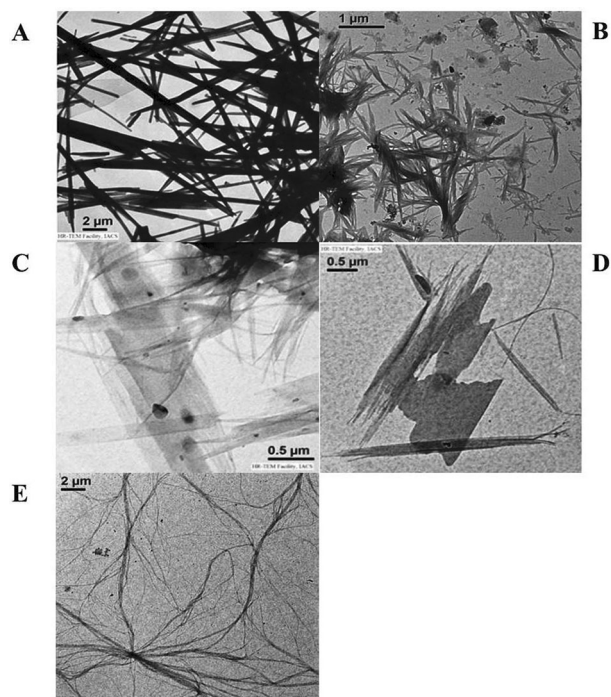


Figure 5. HRTEM images: A) MS gel of **IND-HYP-AMN**. B) MS gel of **IND-LEU-AMN**. C) Chlorobenzene gel of **IND-PHE-AMN**. D) *o*-Xylene gel of **IND-PHE-AMN**. E) Hydrogel of **IND-LEU-AMN**.

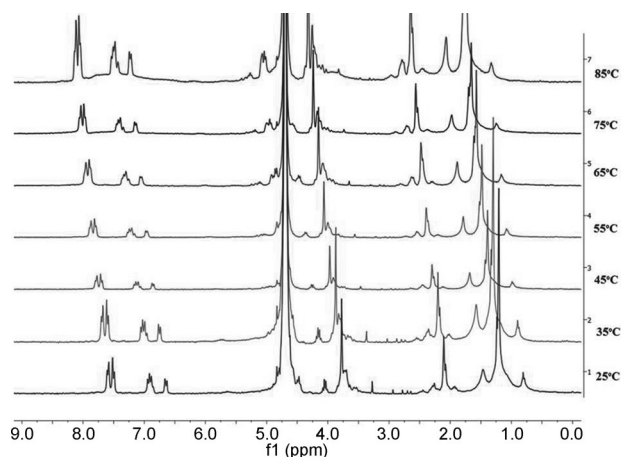


Figure 6. Variable-temperature ^1H NMR spectra of **IND-LEU-AMN** in D_2O .

To understand the supramolecular process of hydrogelation by **IND-LEU-AMN**, we undertook detailed FTIR studies. For this purpose, we considered monitoring the C=O stretching frequency of various hydrogen-bond functionalities such as COOH, CON (tertiary amide) and CONH (secondary amide) present in the drug **IND**, the peptide conjugate **IND-LEU** and the gelator salt **IND-LEU-AMN** (Table 1). The data clearly indicated that both amide moieties in the gelator salt were involved in hydrogen-bonding interactions in the corresponding D_2O gel. It is, however, difficult to propose the exact details of the hydrogen bonding. In most likelihood, both amide C=O groups were involved in N-H...O-type hydrogen bonding,

Table 1. FTIR C=O stretching frequencies [cm^{-1}].			
Compound	COOH	CON (tertiary amide)	CONH (secondary amide)
IND	1716	1691	not applicable
IND-LEU	1733	1683	1652
IND-LEU-AMN	absent	1683	1649
IND-LEU-AMN (D_2O gel)	absent	1620	1606
IND-LEU-AMN ($[\text{D}_6]\text{DMSO}$ sol)	absent	1687	1637

wherein N-H can be amide N-H or ammonium N-H. Interestingly, the absence of the hydrogen-bonded amide band (1620 and 1606 cm^{-1} in the gel) in the molecularly dissolved gelator salt in $[\text{D}_6]\text{DMSO}$ clearly indicated that the C=O groups of the amides were no longer involved in N-H...O hydrogen bonding; instead, the S=O group of $[\text{D}_6]\text{DMSO}$ now took part in hydrogen bonding with the N-H group of the amide and ammonium moieties (see the Supporting Information, Figure S33).

To probe the aggregation process during gelation, we carried out concentration-dependent dynamic light scattering (DLS) experiments on the hydrogelator salt. For this purpose, we scanned an aqueous solution of the gelator salt having various concentrations ranging from below and much above the MGC. The particle sizes of the scatterers at the MGC and at a much higher concentration (2 wt%) were about 5 and about 8 μm , respectively. The data indicated that the size of the scattering particles in such solutions increased with increasing concentration, an observation commensurate with the expected self-assembly process during gelation (Figure 7).

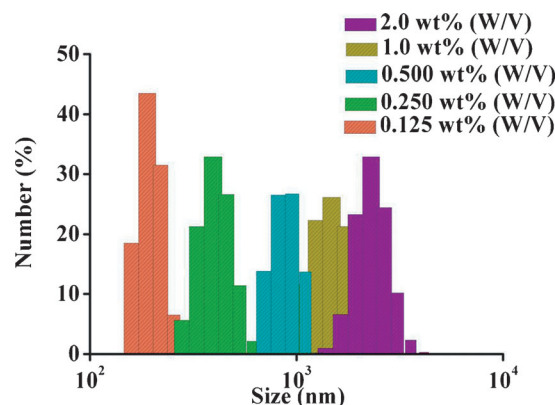


Figure 7. DLS studies on **IND-LEU-AMN** in water (mean with \pm standard deviation error bar).

Since the design aspect of the peptide conjugate salts was based on the assumption that various hydrogen-bond functionalities such as amide and ammonium carboxylate would display orthogonal hydrogen bonding, it was necessary at this stage to determine the single-crystal structure of the gelators studied herein. We obtained X-ray-quality single crystals of **IND-PHE-AMN** and **IND-HYP-AMN**. We could not, however, crystallize the hydrogelator salt. As expected, both salts crystallized in a chiral space group (see the Supporting Information,

Table S2) because of the inherent chirality of the amino acid moiety. Unfortunately, both the crystals picked up lattice-occluded water molecules of solvation and, since water is an excellent hydrogen-bond donor and acceptor, it participated in hydrogen-bonding and thereby disrupted the expected orthogonal hydrogen bonding. In both salts, the 3° amide part of the drug moiety did not participate in hydrogen bonding, whereas the peptide moiety took part in hydrogen bonding with $\text{NH}_3^+/\text{OMe}/\text{water}$ in **IND-PHE-AMN** and $\text{water}/\text{OH}(\text{hydroxyproline})$ in **IND-HYP-AMN**. The COO^- group in both salts was found to be involved in hydrogen bonding with $\text{NH}_3^+/\text{water}$, which prevents PAM-synthon formation. Interestingly, $\text{C-H}\cdots\pi$ interactions (see the Supporting Information, Figures S36 and S37) involving both aromatic and non-aromatic moieties were observed in these salts. Overall, both salts displayed 2D hydrogen-bonded networks (Figure 8).

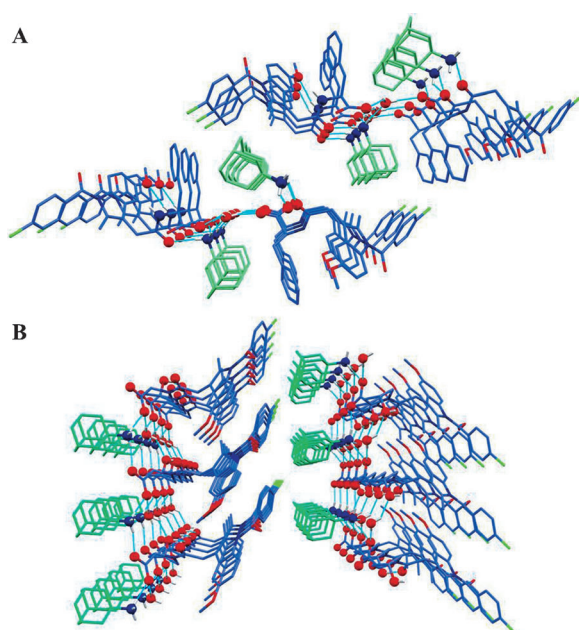


Figure 8. Single-crystal structures of A) **IND-PHE-AMN** and B) **IND-HYP-AMN**.

Since **IND-LEU-AMN** was found to be an ambidextrous gelator and was able to gel efficiently solvents useful in bio-applications (MS and water), we concentrated our focus on this gelator salt. First, we evaluated the ability of this gelator salt to form gels under physiological conditions, which is important for using this modified drug salt for self-delivery applications. The hydrogelator **IND-LEU-AMN** was examined for gelation in saline water (0.9 wt% NaCl solution) and phosphate buffer solution (PBS) at physiological pH 7.4, and in both the cases it was able to form gel with slightly higher MGC (0.75 wt% for 0.9 wt% NaCl solution and 1 wt% for PBS). This could be attributed to the fact that the salts (NaCl and PBS) increased the polarity of the medium and thus resulted in a higher MGC of the gelator by increasing its solubility.

Since the solubility of NSAIDs is a major concern regarding their delivery, we assessed the solubility of the modified pep-

tide-conjugate salt in water. The hydrogelator salt was 78 times more soluble than the parent drug **IND** (see the Supporting Information, Table S5).

Before performing an MTT (3-(4,5-dimethylthiazol-2-yl)-2,5-diphenyltetrazolium bromide) assay,^[66] the stability of the hydrogelator was checked in PBS (pH 7.4) at 37 °C by incubation for 48 h. No degradation in the incubated soup was detected by UV/Vis spectroscopy (see the Supporting Information, Figure S39).

Biocompatibility of the hydrogelator (**IND-LEU-AMN**) as well as of the parent drug (**IND**) is important for determining the concentration of the drug for treating mouse macrophage cells. It was determined by an MTT assay in which the hydrogelator was incubated with mouse macrophage cells (RAW 264.7 cell line) for 24, 48 and 72 h at 37 °C. Both the parent drug and the hydrogelator salt have IC_{50} values greater than 0.50 mM, and the hydrogelator showed better biocompatibility than the parent drug (Figure 9).

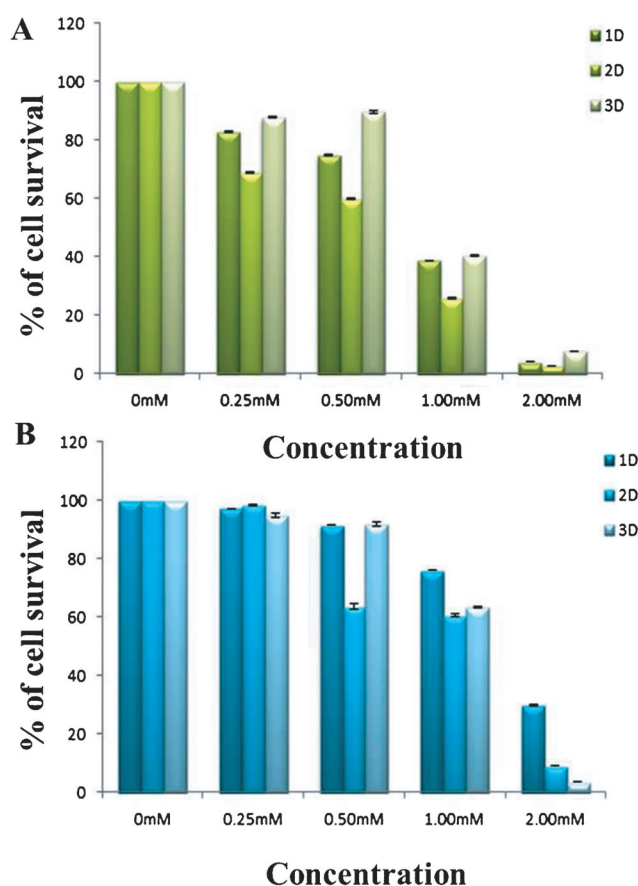


Figure 9. MTT assay of A) **IND** and B) **IND-LEU-AMN** in RAW 264.7 cells for 24, 48 and 72 h at 37 °C. 1D, 2D and 3D stand for 1, 2 and 3 d, respectively.

After determining the biocompatibility of the hydrogel, the anti-inflammatory activity was evaluated by prostaglandin E_2 assay^[67] (PGE_2 assay) in the RAW 264.7 cell line. In this experiment, the maximum inflammation response, which was determined by monitoring the production of PGE_2 in the cell culture

medium, was found by adjusting the amount of inflammation-inducing agents such as lipopolysaccharide (LPS) and interferon gamma (IFN- γ). Concentrations of $1\text{ }\mu\text{g mL}^{-1}$ LPS and 100 ng mL^{-1} IFN- γ produced the maximum of 2012.3 pg mL^{-1} PGE₂ in the RAW 264.7 cell culture medium, which was reduced significantly to 138.7 and 147.6 pg mL^{-1} in the presence of 0.3 mM ($<IC_{50}$) of **IND** and **IND-LEU-AMN**, respectively. These reductions in PGE₂ levels (6.8 and 7.3% for **IND** and **IND-LEU-AMN** respectively) signified that the hydrogelator showed an anti-inflammatory response almost comparable to that of the parent drug **IND** (Figure 10).

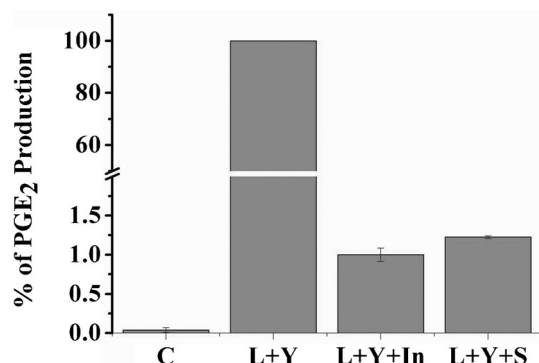


Figure 10. PGE₂ assay of **IND** and **IND-LEU-AMN**. In = indomethacin, L = lipopolysaccharide, Y = interferon- γ and S = **IND-LEU-AMN**.

To establish the multidrug self-delivery capability of the hydrogelator in drug-delivery applications, a leaching experiment on the hydrogel of **IND-LEU-AMN** was performed under physiological conditions (PBS, pH 7.4 at 37°C) by placing $100\text{ }\mu\text{L}$ of PBS (pH 7.4) over $100\text{ }\mu\text{L}$ of a 4 wt% hydrogel in a test tube. Five such test tubes were incubated at 37°C for various time intervals (3, 6, 9, 12 and 24 h) in each case. The concentration of the gelator in the PBS layer was determined in triplicate by UV spectrophotometry. The hydrogel showed a maximum leaching of 36% after 24 h. Thus, it can be concluded that the hydrogel could be used as a useful tool in self-delivery applications (see the Supporting Information, Figure S40).

To carry out cell imaging, it was necessary to evaluate the emission behaviour of **IND-LEU-AMN** in aqueous solution. The emission spectra of the sol and gel of **IND-LEU-AMN** in double-distilled water (4.0 wt% for both sol and gel) showed a significant increase in the emission intensity on going from sol to gel at approximately 450 nm ($\lambda = 329\text{ nm}$), which could be attributed to aggregation-induced emission (see the Supporting Information, Figure S34).^[68,69] This result encouraged us to further explore the possibility of using the drug gelator salt for cell imaging. For this purpose, we chose to work with the RAW 264.7 cell line (see the Experimental Section for details). Figure 11 shows the bright-field, fluorescence and overlay images of cells exposed to the gelator drug. The considerable background in Figure 11B could be due to weak autofluorescence (see the Supporting Information, Figure S41) and also because of phagocytosis.^[70] However, localization of fluorescence in Figure 11C clearly indicated penetration of the gelator

drug. The most conclusive evidence came from Z-stacking (see the Supporting Information for a video). Thus, it was clear that the gelator salt indeed penetrated the cell membrane and adequately accumulated within the cells to give emission in the green region (Figure 11).

Conclusion

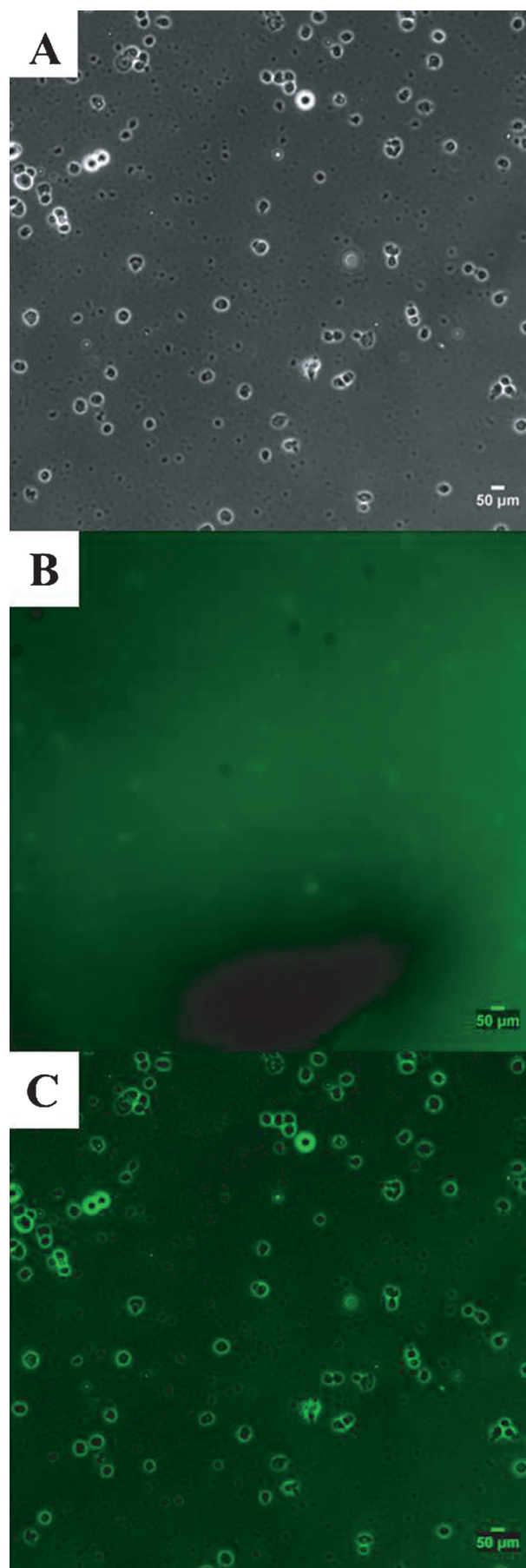
By exploiting covalent and supramolecular approaches, a new series of organic salt based supramolecular gelators derived from two different drugs (indomethacin and amantadine) was designed. Half of the organic salts thus synthesized showed versatile gelation ability. One such ambidextrous gelator, namely, **IND-LEU-AMN**, was found to be biocompatible (MTT assay), anti-inflammatory (PGE₂ assay) and capable of cell imaging. The hydrogel of this salt was injectable and hence could possibly be used for self-delivery purposes via invasive (subcutaneous) and non-invasive (topical) routes. The MS organogel of this salt exhibited intriguing materials properties, which included shape sustaining, load-bearing and self-healing behaviour. The results clearly indicated that the strategy adopted herein could be used in developing multidrug-based supramolecular gelators for combination therapy.

Experimental Section

Materials: All chemicals were commercially available and used without further purification. Solvents were of analytical-reagent grade and used without further distillation. PGE₂ assay was performed by using Prostaglandin E2 EIA Kit - Monoclonal (Cayman Chemicals, Ann Arbor, MI).

Methods: Melting points of all the salts were determined with a programmable melting point apparatus (Veego, India). The elemental analyses of the salts were carried out with a PerkinElmer 2400 Series II CHNO/S Elemental Analyzer. The mass spectra were collected with a QTOF Micro YA263 instrument. FTIR spectra were obtained with a Shimadzu FTIR-8300 instrument. ^1H and ^{13}C NMR spectra were recorded with a 300 MHz spectrometer (Bruker Ultra-shield Plus-300). TEM images were recorded with a JEOL instrument on 300 mesh copper TEM grids. SEM images were recorded with a JEOL JMS-6700F field-emission scanning electron microscope. Rheology studies were carried out with an Anton Paar Modular Compact Rheometer MCR 102. Emission spectra were recorded with a Fluorolog Horiba Jobin Yvon Fluoromax 4C Fluorescence Spectrometer. A JASCO J-815 CD spectrometer was used to carry out circular dichroism experiments. Differential scanning calorimetry was done with a PerkinElmer Pyris Diamond DSC. Dynamic light scattering experiments were executed with a Malvern Particle Size Analyzer (Model No. ZEN 3690 ZETASIZER NANO ZS 90 version 7.03). A VARIAN CARY 50 Bio UV-Visible Spectrophotometer was used to measure the concentration of the hydrogelator in biostability and leaching experiments. MTT and PGE₂ assays were conducted by using a multiplate ELISA reader (Varioskan Flash Elisa Reader, Thermo Fisher).

X-ray diffraction: Single-crystal X-ray diffraction data were collected by using $\text{Mo K}\alpha$ ($\lambda = 0.7107\text{ \AA}$) radiation with a Bruker APEX II diffractometer equipped with CCD area detector. A Bruker AXS D8 Advance powder diffractometer equipped with super speed LYNXEYE detector ($\text{Cu K}\alpha_1$ radiation, $\lambda = 1.5406\text{ \AA}$, scan speed =



0.3 s step⁻¹, step size = 0.02°) was used to collect powder XRD data.

Synthesis of salts: All the salts were prepared by reaction of the corresponding acids and amines in 1:1 molar ratio in methanol at room temperature followed by evaporation of the solvent in a rotary evaporator (see the Supporting Information, Scheme S2). The resultant solid was isolated as the salt in near-quantitative yield. FTIR spectra (KBr) of the salts showed the presence of stretching band of the carboxylate group (COO) at 1683–1680 cm⁻¹ and the absence of the carbonyl stretching band (C=O) of the COOH group at 1735–1712 cm⁻¹ indicating complete salt formation (see the Supporting Information, Figure S1).

Synthesis of peptides: Indomethacin (3.0 mmol, 1073.37 mg) and *N*-hydroxysuccinimide (3.3 mmol, 379.797 mg) were placed in a two-neck round-bottom flask and dissolved in dry THF (50 mL) to form a homogeneous solution. The reaction mixture was stirred for 10 min in an ice bath (0–5 °C) under argon atmosphere, and then a solution of dicyclohexylcarbodiimide (4.5 mmol, 928.485 mg) in dry THF (20 mL) was added dropwise. The reaction mixture was stirred overnight at room temperature. The white precipitate obtained was filtered off and the filtrate was concentrated under reduced pressure. After evaporation of the solvent, the residue was again dissolved in 60 mL THF and then corresponding L-amino acid (3.0 mmol) dissolved in aqueous sodium carbonate (2.4 mmol, 254.372 mg) was added and the mixture stirred for 24 h. THF was removed under reduced pressure and then the solution was acidified with cold aqueous HCl (1 N) in a dropwise manner to obtain a white precipitate. The precipitate was collected by filtration and washed with distilled water to remove the excess acid. The solid product thus obtained was dried in a vacuum desiccator and purified by column chromatography (2% MeOH in CH₂Cl₂) to give 73–82% of pure product (see the Supporting Information, Scheme S1).

Physicochemical Data

IND-PHE-AM: Light yellow solid, m.p. 173–174 °C; elemental analysis calcd (%) for C₃₈H₄₂ClN₃O₅: C 69.55, H 6.45, N 6.40; found: C 69.91, H 6.25, N 6.76; ¹H NMR (300 MHz, [D₄]methanol, 25 °C): δ = 7.63–7.55 (d, *J* = 8.6 Hz, 2H), 7.55–7.48 (d, *J* = 8.7 Hz, 2H), 7.10–7.04 (d, *J* = 9.0 Hz, 1H), 7.04–6.98 (s, 5H), 6.98–6.94 (d, *J* = 2.6 Hz, 1H), 6.74–6.66 (dd, *J* = 2.9, 2.6 Hz, 1H), 4.54–4.41 (t, *J* = 5.7 Hz, 1H), 3.84–3.72 (s, 3H), 3.63–3.50 (m, 2H), 3.20–3.07 (dd, *J* = 5.9, 4.9 Hz, 1H), 3.07–2.90 (dd, *J* = 6.0, 6.4 Hz, 1H), 2.18–2.02 (d, *J* = 12.7 Hz, 6H), 1.86–1.60 ppm (m, 11H); ¹³C NMR (75 MHz, [D₄]methanol): δ = 170.5, 170.4, 168.4, 156.3, 138.6, 137.5, 136.3, 135.4, 134.2, 131.0, 130.9, 130.6, 129.1, 128.7, 127.6, 127.5, 125.7, 114.5, 113.2, 111.6, 100.8, 55.5, 54.7, 51.2, 48.1, 40.0, 37.3, 34.9, 31.0, 28.9, 12.2 ppm (Supporting Information, Figure S2); FTIR (KBr pellet): 1680 cm⁻¹ (s, salt carboxylate C=O stretch).

IND-HYP-AMN: Light yellow solid, m.p. 177–178 °C; elemental analysis calcd (%) for C₃₄H₄₀ClN₃O₆·CH₃OH: C 64.26, H 6.78, N 6.42; found: C 64.81, H 6.29, N 6.76; ¹H NMR (300 MHz, [D₄]methanol, 25 °C): δ = 7.78–7.61 (dd, *J* = 8.4, 9.0 Hz, 2H), 7.61–7.44 (m, 2H), 7.10–6.98 (dd, *J* = 3.0, 2.6 Hz, 1H), 6.99–6.86 (m, 1H), 4.65–4.44 (m, 1H), 3.91–3.73 (m, 4H), 3.73–3.48 (m, 3H), 2.45–2.29 (m, 1H), 2.28–2.16 (d, *J* = 8.1 Hz, 3H), 2.16–2.06 (m, 4H), 1.91–1.58 ppm (m, 13H); ¹³C NMR (75 MHz, [D₄]methanol): δ = 172.7, 171.1, 167.0, 155.9, 135.1, 134.5, 132.2, 130.8, 130.7, 130.6, 128.7, 128.4, 123.7, 123.3, 114.3, 110.4, 109.5, 103.4, 100.9, 98.9, 69.4, 54.9, 54.7, 51.1, 40.2,

Figure 11. Fluorescent microscopy images of the RAW 264.7 cells incubated with the hydrogelator **IND-LEU-AMN**. A) bright field, B) fluorescence and C) overlay images.

37.6, 35.0, 28.9, 12.2, 10.3 ppm (Supporting Information, Figure S3); FTIR (KBr pellet): 1683 cm^{-1} (s, salt carboxylate C=O stretch).

IND-LEU-AMN: Light yellow solid, m.p. 167–168 °C; elemental analysis calcd (%) for $\text{C}_{35}\text{H}_{44}\text{ClN}_3\text{O}_5$: C 67.56, H 7.13, N 6.75; found: C 68.01, H 6.68, N 6.79; ^1H NMR (300 MHz, $[\text{D}_4]$ methanol, 25 °C): δ = 7.78–7.62 (d, J = 8.3 Hz, 2H), 7.62–7.44 (d, J = 8.4 Hz, 2H), 7.14–6.86 (m, 2H), 6.76–6.55 (dd, J = 3.0, 2.6 Hz, 1H), 4.44–4.24 (dd, J = 3.0, 3.9 Hz, 1H), 3.89–3.71 (s, 3H), 3.71–3.56 (d, J = 2.2 Hz, 2H), 2.38–2.20 (s, 3H), 2.20–2.00 (t, J = 3.4 Hz, 3H), 1.94–1.36 (m, 16H), 1.02–0.66 ppm (d, J = 5.8 Hz, 6H); ^{13}C NMR (75 MHz, $[\text{D}_4]$ methanol): δ = 170.7, 170.1, 168.4, 156.2, 138.6, 138.0, 135.5, 134.3, 130.9, 128.7, 114.5, 113.5, 111.5, 100.8, 54.6, 53.5, 51.0, 42.0, 40.2, 35.0, 33.3, 31.0, 28.9, 24.7, 22.3, 20.9, 12.2 ppm (Supporting Information, Figure S4); FTIR (KBr pellet): 1683 cm^{-1} (s, salt carboxylate C=O stretch).

IND-VAL-AMN: Light yellow solid, m.p. 161–162 °C; elemental analysis calcd (%) for $\text{C}_{34}\text{H}_{42}\text{ClN}_3\text{O}_5$: C 67.15, H 6.96, N 6.91; found: C 67.66, H 7.34, N 7.19; ^1H NMR (300 MHz, $[\text{D}_4]$ methanol, 25 °C): δ = 7.78–7.61 (d, J = 8.4 Hz, 2H), 7.61–7.45 (d, J = 8.6 Hz, 2H), 7.13–7.01 (d, J = 2.5 Hz, 1H), 7.01–6.87 (d, J = 9.1 Hz, 1H), 6.77–6.58 (dd, J = 3.0, 2.6 Hz, 1H), 4.33–4.09 (d, J = 4.8 Hz, 1H), 3.87–3.72 (s, 3H), 3.72–3.54 (d, J = 3.2 Hz, 2H), 2.40–2.20 (s, 3H), 2.21–2.04 (m, 3H), 1.94–1.55 (m, 9H), 0.96–0.86 (d, J = 6.9 Hz, 3H), 0.87–0.75 ppm (d, J = 6.9 Hz, 3H); ^{13}C NMR (75 MHz, $[\text{D}_4]$ methanol): δ = 171.0, 170.9, 170.0, 156.2, 138.6, 135.5, 134.3, 130.9, 130.6, 128.7, 125.0, 114.5, 113.5, 112.8, 111.6, 100.7, 59.9, 54.7, 51.2, 40.1, 34.9, 31.3, 31.1, 28.9, 18.7, 16.8, 12.2 ppm (Supporting Information, Figure S5); FTIR (KBr pellet): 1683 cm^{-1} (s, salt carboxylate C=O stretch).

IND-ALA-AMN: Light yellow solid, m.p. 158–159 °C; elemental analysis calcd (%) for $\text{C}_{32}\text{H}_{38}\text{ClN}_3\text{O}_5 \cdot \text{H}_2\text{O}$: C 64.26, H 6.74, N 7.03; found: C 63.94, H 7.14, N 7.22; ^1H NMR (300 MHz, $[\text{D}_4]$ methanol, 25 °C): δ = 7.75–7.65 (d, J = 8.5 Hz, 2H), 7.61–7.51 (d, J = 8.5 Hz, 2H), 7.06–7.00 (d, J = 2.6 Hz, 1H), 7.00–6.93 (d, J = 9.0 Hz, 1H), 6.71–6.63 (dd, J = 2.4, 2.5 Hz, 1H), 4.32–4.13 (q, J = 7.1 Hz, 1H), 3.85–3.73 (s, 3H), 3.69–3.58 (s, 2H), 2.33–2.23 (s, 3H), 2.22–2.04 (d, J = 2.8 Hz, 3H), 1.92–1.56 (m, 9H), 1.41–1.27 ppm (d, J = 7.0 Hz, 3H); ^{13}C NMR (75 MHz, $[\text{D}_4]$ methanol): δ = 177.2, 174.2, 168.5, 156.0, 138.4, 134.6, 134.3, 131.5, 130.9, 130.8, 128.6, 115.9, 114.3, 110.9, 108.9, 101.3, 58.4, 54.6, 51.2, 40.0, 36.1, 34.9, 32.3, 28.9, 12.2 ppm (Supporting Information, Figure S6); FTIR (KBr pellet): 1683 cm^{-1} (s, salt carboxylate C=O stretch).

IND-THR-AMN: Yellow solid, m.p. 171–172 °C; elemental analysis calcd (%) for $\text{C}_{33}\text{H}_{40}\text{ClN}_3\text{O}_6 \cdot \text{CH}_3\text{OH}$: C 63.59, H 6.91, N 6.54; found: C 63.94, H 7.14, N 7.22; ^1H NMR (300 MHz, $[\text{D}_4]$ methanol, 25 °C): δ = 7.79–7.62 (d, J = 8.5 Hz, 2H), 7.62–7.44 (d, J = 8.5 Hz, 2H), 7.12–6.92 (m, 2H), 6.74–6.60 (dd, J = 2.4, 2.5 Hz, 1H), 4.33–4.24 (d, J = 3.3 Hz, 1H), 4.24–4.12 (m, 1H), 3.90–3.75 (s, 3H), 3.75–3.61 (d, J = 2.9 Hz, 2H), 2.43–2.22 (s, 3H), 2.22–2.01 (t, J = 3.1 Hz, 3H), 1.97–1.53 (m, 10H), 1.17–0.95 (d, J = 6.3 Hz, 3H) ppm; ^{13}C NMR (75 MHz, $[\text{D}_4]$ methanol): δ = 173.5, 172.3, 168.7, 156.2, 138.6, 135.5, 134.4, 130.9, 130.6, 128.7, 128.4, 114.8, 111.7, 108.2, 100.7, 67.5, 56.0, 54.7, 50.4, 40.2, 35.0, 31.0, 28.9, 18.6, 12.2 ppm (Supporting Information, Figure S7); FTIR (KBr pellet): 1681 cm^{-1} (s, salt carboxylate C=O stretch).

Hydrogel gelation and T_{gel} experiments: to prepare hydrogels, we first dissolved the gelator in pure water by heating, and the hot clear solution was then allowed to cool to room temperature to afford a stable hydrogel within a few minutes. Hydrogel formation was confirmed by test-tube inversion. The T_{gel} values of the four hydrogels were measured (only for pure-water gels) by the dropping-ball method at various gelator concentrations. A glass ball weighing 205.50 mg was placed on 0.5 mL of hydrogel (at the respective MGC) in a test tube (15 × 100 mm). The test tube was then immersed in an oil bath placed on a magnetic stirrer to

ensure uniform heating. The temperature at which the ball touched the bottom of the test tube was noted (see the Supporting Information, Figures S11 and S12).

Organogel gelation and T_{gel} experiments: To prepare organogels, we first dissolved the gelator in organic solvent by heating, and the hot clear solution was then allowed to cool to room temperature to afford a stable organogel within a few minutes. Organogel formation was confirmed by test-tube inversion. The T_{gel} values of the organogels were measured by the dropping-ball method at various gelator concentrations. A glass ball weighing 205.50 mg was placed on 0.5 mL of organogel (at the MGC) in a test tube (15 × 100 mm). The test tube was then immersed in an oil bath placed on a magnetic stirrer to ensure uniform heating. The temperature at which the ball touched the bottom of the test tube was noted (see the Supporting Information, Figures S11 and S12).

SEM and TEM sample preparation: Dilute (0.1 wt%) solutions of the gelators were drop cast on a glass plate with attached standard metallic SEM stub and dried under ambient conditions. The samples were coated with platinum, and the SEM images were recorded. Dilute (0.1 wt%) solutions of the gelators were drop cast on a carbon-coated Cu TEM grid (300 mesh) for each sample. The grid was dried under vacuum at room temperature for 1 d and used for recording TEM images at an accelerating voltage of 200 kV without staining.

Rheology studies: Rheology studies were carried out with an Anton Paar Modular Compact Rheometer MCR 102 on 4 wt% gels at 25 °C in parallel-plate geometry (25 mm diameter, 1 mm gap).

Single crystal X-ray diffraction: Single crystals of **IND-PHE-AMN** and **IND-HYP-AMN** were grown from pure methanol as solvent by slow evaporation at room temperature. Data were collected by using $\text{Mo}_{\text{K}\alpha}$ (λ = 0.7107 Å) radiation with a Bruker APEX II diffractometer equipped with CCD area detector. Data collection, data reduction and structure solution/refinement were carried out with the SMART APEX-II software package. All structures were solved by direct methods and refined in a routine manner. Non-hydrogen atoms were treated anisotropically. All hydrogen atoms were geometrically fixed. CCDC 1480781 (**IND-PHE-AMN**), and 1480782 (**IND-HYP-AMN**) contain the supplementary crystallographic data for this paper. These data are provided free of charge by The Cambridge Crystallographic Data Centre.

MTT assay: The cytotoxicity of the gelator salt was evaluated in RAW 264.7 cells by standard MTT assay. The mouse macrophage RAW 264.7 cells were purchased from American Type Culture Collection (ATCC) and maintained by following its guidelines. The cells were grown in Dulbecco's modified Eagle's medium (DMEM) supplemented with 10% fetal bovine serum (FBS), 1% penicillin and streptomycin in a humidified incubator at 37 °C and 5% CO_2 . The cells were seeded in 96-well plates at a density of 1×10^4 cells/well for 24 h. After 24 h of seeding, the cells were treated with various concentrations (up to 2 mM) of the salt or DMEM alone for 72 h in a humidified incubator at 37 °C and 5% CO_2 . Then, the culture medium was replaced with 100 μg of MTT per well and kept for 4 h at 37 °C. To dissolve the formazan produced by mitochondrial reductase from live cells, DMSO (100 μL /well) was added and the medium incubated for 30 min at room temperature. The colour intensity of the formazan solution, which is positively correlated to the cell viability, was measured with a multiplate ELISA reader at 570 nm (Varioskan Flash Elisa Reader, Thermo Fisher). The percentage of live cells in salt-treated samples was calculated by considering the DMEM-treated sample as 100%. This experiments were done in triplicate.

PGE₂ assay: Production of PGE₂ was estimated according to a published protocol^[67] by using six-well plates and the RAW 264.7 cell line. Approximately 1×10^6 cells/well were seeded in four wells of six-well plates for 24 h. One of the wells was treated with 2 mL of DMEM alone as control experiment, and the remaining three wells were treated with $1 \mu\text{g mL}^{-1}$ lipopolysaccharide (LPS) and 100 ng mL^{-1} interferon gamma (IFN- γ); two of these LPS/IFN- γ -treated wells were treated with 0.3 mM IND and IND-LEU-AMN, respectively, in such a way that the total medium (DMEM) volume in each well was 2 mL, and all the wells were further incubated for 24 h. The culture medium was diluted to 1:100 or 1:500 for measuring PGE₂ with Prostaglandin E₂ EIA Kit - Monoclonal (Cayman Chemicals, Ann Arbor, MI). This experiment was done in triplicate.

Cell imaging: Having successfully established the biocompatibility of the hydrogel, it was applied in cell imaging. RAW 264.7 cells were cultured by using DMEM supplemented with 10% FBS and 1% penicillin/streptomycin on ethanol-etched cover slips kept in 35 mm tissue-culture dishes. These were kept in a humidified incubator at 37 °C overnight. Then the medium was removed and fresh hydrogelator-containing medium was added (5 mM). The medium was incubated for 30 min. Then, the medium was removed and fresh medium was added. The cells were mounted on a confocal Petri dish, and a Carl Zeiss Axio Observer Z1 microscope fitted with a Hamamatsu Orca-Flash4.0 digital camera was used to acquire the images.

Acknowledgements

P.D. thanks DBT, DST and IACS New Delhi for financial support (CEIB project BT/01/CEIB/V/13). R.R. thanks CSIR, New Delhi, for SRF (CSIR grant no. 09/080(0802)/2012-EMR-I). SXR data were collected at the DBT-funded X-ray diffraction facility under the CEIB program in the Department of Organic Chemistry, IACS, Kolkata. We thank Mahesh Agarwal of Department of Biological Chemistry, IACS for fluorescence microscopy images; Biplab Kumar Patra of Department of Materials Science, IACS for collecting the PL data; and Dr. Ahmad Husain and Dr. Suman Bhattacharya of Department of Organic Chemistry for crystallographic discussions.

Keywords: drug delivery • gels • hydrogen bonds • imaging agents • supramolecular chemistry

- [1] F. Zhao, M. L. Ma, B. Xu, *Chem. Soc. Rev.* **2009**, 38, 883–891.
- [2] X. Du, J. Zhou, J. Shi, B. Xu, *Chem. Rev.* **2015**, 115, 13165–13307.
- [3] E. Carretti, L. Dei, R. G. Weiss, *Soft Matter* **2005**, 1, 17–22.
- [4] L. Yu, J. Ding, *Chem. Soc. Rev.* **2008**, 37, 1473–1481.
- [5] V. Gujrati, S. Kim, S.-H. Kim, J. J. Min, H. E. Choy, S. C. Kim, S. Jon, *ACS Nano* **2014**, 8, 1525–1537.
- [6] B. Lukanov, A. Firoozabadi, *Langmuir* **2016**, 32, 3100–3109.
- [7] B. S. Bolu, E. M. Gecici, R. Sanyal, *Mol. Pharm.* **2016**, 13, 1482–1490.
- [8] Z. Zhang, X. Zhang, X. Xu, Y. Li, Y. Li, D. Zhong, Y. He, Z. Gu, *Adv. Funct. Mater.* **2015**, 25, 5250–5260.
- [9] R. Langer, *Nature* **1998**, 392, 5–10.
- [10] K. E. Uhrich, S. M. Cannizzaro, R. S. Langer, K. M. Shakesheff, *Chem. Rev.* **1999**, 99, 3181–3198.
- [11] M. J. Webber, J. B. Matson, V. K. Tamboli, S. I. Stupp, *Biomaterials* **2012**, 33, 6823–6832.
- [12] J. Li, Y. Gao, Y. Kuang, J. Shi, X. Du, J. Zhou, H. Wang, Z. Yang, B. Xu, *J. Am. Chem. Soc.* **2013**, 135, 9907–9914.
- [13] H. Wang, J. Wei, C. Yang, H. Zhao, D. Li, Z. Yin, Z. Yang, *Biomaterials* **2012**, 33, 5848–5853.
- [14] Z. Yang, K. Xu, L. Wang, H. Gu, H. Wei, M. Zhang, B. Xu, *Chem. Commun.* **2005**, 4414–4416.
- [15] R. Lin, A. G. Cheetham, P. Zhang, Y. Lin, H. Cui, *Chem. Commun.* **2013**, 49, 4968–4970.
- [16] H. Wang, Z. Yang, *Soft Matter* **2012**, 8, 2344–2347.
- [17] R. V. Ulijn, A. M. Smith, *Chem. Soc. Rev.* **2008**, 37, 664–675.
- [18] P. K. Vemula, U. Aslam, V. A. Mallia, G. John, *Chem. Mater.* **2007**, 19, 138–140.
- [19] J. W. Steed, *Chem. Soc. Rev.* **2010**, 39, 3686–3699.
- [20] P. Terech, R. G. Weiss, *Chem. Rev.* **1997**, 97, 3133–3160.
- [21] D. J. Abdallah, R. G. Weiss, *Adv. Mater.* **2000**, 12, 1237–1247.
- [22] J. A. Foster, M. M. Piepenbrock, G. O. Lloyd, N. Clarke, J. A. K. Howard, J. W. Steed, *Nat. Chem.* **2010**, 2, 1037–1043.
- [23] J. J. D. de Jong, L. N. Lucas, R. M. Kellogg, J. H. van Esch, B. L. Feringa, *Science* **2004**, 304, 278–281.
- [24] A. Wynne, M. Whitefield, A. J. Dixon, S. Anderson, *J. Dermatol. Treat.* **2002**, 13, 61–66.
- [25] S. S. Babu, V. K. Praveen, A. Ajayaghosh, *Chem. Rev.* **2014**, 114, 1973–2129.
- [26] A. P. Piccionello, A. Guarcello, A. Calabrese, I. Pibiri, A. Pace, S. Buscemia, *Org. Biomol. Chem.* **2012**, 10, 3044–3052.
- [27] B. Escuder, F. Rodriguez-Llansola, J. F. Miravet, *New J. Chem.* **2010**, 34, 1044–1054.
- [28] E. Carretti, E. Fratini, D. Berti, L. Dei, P. Baglioni, *Angew. Chem. Int. Ed.* **2009**, 48, 8966–8969; *Angew. Chem.* **2009**, 121, 9128–9131.
- [29] R. N. Shah, N. A. Shah, M. M. D. R. Lim, C. Hsieh, G. Nuber, S. I. Stupp, *Proc. Natl. Acad. Sci. USA* **2010**, 107, 3293–3298.
- [30] K. J. C. van Bommel, A. Friggeri, S. Shinkai, *Angew. Chem. Int. Ed.* **2003**, 42, 980–999; *Angew. Chem.* **2003**, 115, 1010–1030.
- [31] Z. A. C. Schneppe, R. Gonzalez-McQuire, S. Mann, *Adv. Mater.* **2006**, 18, 1869–1872.
- [32] Z. Yang, G. Liang, M. Ma, A. S. Abbah, W. W. Lu, B. Xu, *Chem. Commun.* **2007**, 843–845.
- [33] Q. Wang, Z. Yang, X. Zhang, X. Xiao, C. K. Chang, B. Xu, *Angew. Chem. Int. Ed.* **2007**, 46, 4285–4289; *Angew. Chem.* **2007**, 119, 4363–4367.
- [34] S. Kiyonaka, K. Sada, I. Yoshimura, S. Shinkai, N. Kato, I. Hamachi, *Nat. Mater.* **2004**, 3, 58–64.
- [35] K. Y. Lee, D. J. Mooney, *Chem. Rev.* **2001**, 101, 1869–1879.
- [36] S. M. Standley, D. J. Toft, H. Cheng, S. Soukasene, J. Chen, S. M. Raja, V. Band, H. Band, V. L. Cryns, S. I. Stupp, *Cancer Res.* **2010**, 70, 3020–3026.
- [37] F. Zhao, B. A. Heesters, I. Chiu, Y. Gao, J. Shi, N. Zhou, M. C. Carroll, B. Xu, *Org. Biomol. Chem.* **2014**, 12, 6816–6819.
- [38] V. Jayawarna, M. Ali, T. A. Jowitt, A. F. Miller, A. Saiani, J. E. Gough, R. V. Ulijn, *Adv. Mater.* **2006**, 18, 611–614.
- [39] Y. Lan, M. G. Corradini, X. Liu, T. E. May, F. Borondics, R. G. Weiss, M. A. Rogers, *Langmuir* **2014**, 30, 14128–14142.
- [40] M. Suzuki, K. Hanabusa, *Chem. Soc. Rev.* **2009**, 38, 967–975.
- [41] L. Meazza, J. A. Foster, K. Fucke, P. Metrangolo, G. Resnati, J. W. Steed, *Nat. Chem.* **2013**, 5, 42–47.
- [42] O. Lebel, M. Perron, T. Maris, S. F. Zalzal, A. Nanci, J. D. Wuest, *Chem. Mater.* **2006**, 18, 3616–3626.
- [43] M. L. Muro-Small, J. Chen, A. J. McNeil, *Langmuir* **2011**, 27, 13248–13253.
- [44] M. George, R. G. Weiss, *Acc. Chem. Res.* **2006**, 39, 489–497.
- [45] P. Dastidar, *Chem. Soc. Rev.* **2008**, 37, 2699–2715.
- [46] T. K. Adalder, U. K. Das, J. Majumder, R. Roy, P. Dastidar, *J. Indian Inst. Sci.* **2014**, 94:1, 9–24.
- [47] U. K. Das, T. K. Adalder, J. Majumder, R. Roy, P. Dastidar in *Hydrogen Bonded Supramolecular Materials* (Eds.: Z.-T. Li, L.-Z. Wu) **2015**, Chapter 4, pp. 101–131.
- [48] G. R. Desiraju, *Angew. Chem. Int. Ed. Engl.* **1995**, 34, 2311–2327; *Angew. Chem.* **1995**, 107, 2541–2558.
- [49] G. R. Desiraju, J. J. Vittal, A. Ramanan, *Crystal Engineering—A Textbook*, World Scientific, Singapore, **2011**.
- [50] P. Sahoo, R. Sankolli, H.-Y. Lee, S. R. Raghavan, P. Dastidar, *Chem. Eur. J.* **2012**, 18, 8057–8063.
- [51] T. K. Adalder, D. P. Kumar, P. Dastidar, *Cryst. Growth Des.* **2014**, 14, 11–14.
- [52] D. R. Trivedi, A. Ballabh, P. Dastidar, B. Ganguly, *Chem. Eur. J.* **2004**, 10, 5311–5322.


- [53] J. Majumder, J. Deb, M. R. Das, S. S. Jana, P. Dastidar, *Chem. Commun.* **2014**, 50, 1671–1674.
- [54] R. Roy, J. Deb, S. S. Jana, P. Dastidar, *Chem. Asian J.* **2014**, 9, 3196–3206.
- [55] R. Roy, J. Deb, S. S. Jana, P. Dastidar, *Chem. Eur. J.* **2014**, 20, 15320–15324.
- [56] L. A. Estroff, A. D. Hamilton, *Chem. Rev.* **2004**, 104, 1201–1217.
- [57] A. Das, S. Ghosh, *Angew. Chem. Int. Ed.* **2014**, 53, 1092–1097; *Angew. Chem.* **2014**, 126, 1110–1115.
- [58] A. Heeres, C. van der Pol, M. Stuart, A. Friggeri, B. L. Feringa, J. van Esch, *J. Am. Chem. Soc.* **2003**, 125, 14252–14253.
- [59] J. Majumder, P. Dastidar, *Chem. Eur. J.* **2015** in press.
- [60] M. Frenette, G. Cosa, T. Friščić, *CrystEngComm* **2013**, 15, 5100–5106.
- [61] K. Y. Zhang, K. K.-W. Lo, *Inorg. Chem.* **2009**, 48, 6011–6025.
- [62] L. R. Palmera, T. Chen, A. M. I. Lam, D. B. Fenske, K. F. Wong, I. MacLachlan, P. R. Cullis, *Biochim Biophys. Acta* **2003**, 1611, 204–216.
- [63] X. Li, Y. Kuang, H. Lin, Y. Gao, J. Shi, B. Xu, *Angew. Chem. Int. Ed.* **2011**, 50, 9365–9369; *Angew. Chem.* **2011**, 123, 9537–9541.
- [64] S. R. Raghavan, B. H. Cipriano, R. G. Weiss, P. Terech, *Molecular Gels: Materials with Self-Assembled Fibrillar Networks*, **2005**, Springer, Dordrecht, Chapter 8, pp. 233–244.
- [65] J. H. Jung, S. Shinkai, T. Shimizu, *Chem. Eur. J.* **2002**, 8, 2684–2690.
- [66] Q.-S. Wang, Y. Xiang, Y.-L. Cui, K.-M. Lin, X.-F. Zhang, *PLoS One* **2012**, 7, e34122.
- [67] E. Heiss, C. Herhaus, K. Klimo, B. Bartsch, C. Gerhauser, *J. Biol. Chem.* **2001**, 276, 32008–32015.
- [68] Y. Hong, J. W. Y. Lam, B. Z. Tang, *Chem. Soc. Rev.* **2011**, 40, 5361–5388.
- [69] M. R. Molla, S. Ghosh, *Chem. Eur. J.* **2012**, 18, 1290–1294.
- [70] R. J. Anand, S. C. Gribar, J. Li, J. W. Kohler, M. F. Branca, T. Dubowski, C. P. Sodhi, D. J. Hackam, *J. Leukocyte Biol.* **2007**, 82, 1257–1265.

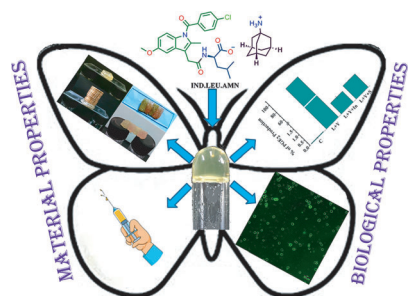
Received: May 21, 2016

Published online on ■ ■ ■, 0000

Imaging Agents

11-11

 **Multidrug-Containing, Salt-Based, Injectable Supramolecular Gels for Self-Delivery, Cell Imaging and Other Materials Applications**



Smart gels: Organic salts derived from peptide conjugates of the non-steroidal anti-inflammatory drug indomethacin (**IND**) and the antiviral drug amantadine (**AMN**) exhibit remarkable gelation ability that makes them suitable for multidrug-self-delivery, cell imaging and other materials applications (see figure; **LEU** = L-leucine).